The CRISPR Journal
Volume 5, Number 1, 2022
Mary Ann Liebert, Inc.
DOI: 10.1089/crispr.2021.0087

The CRISPR Journal

RESEARCH ARTICLE PATH TO THE CLINIC

Chimeric RNA: DNA TracrRNA Improves Homology-Directed Repair *In Vitro* and *In Vivo*

Brandon W. Simone,[1] Han B. Lee,[1] Camden L. Daby,[1] Hirotaka Ata,[2] Santiago Restrepo-Castillo,[3] Gabriel Martínez-Gálvez,[4] Bibekananda Kar,[1] William A.C. Gendron,[3] Karl J. Clark,[1] and Stephen C. Ekker[1,*]

Abstract

Nearly 90% of human pathogenic mutations are caused by small genetic variations, and methods to correct these errors efficiently are critically important. One way to make small DNA changes is providing a single-stranded oligo deoxynucleotide (ssODN) containing an alteration coupled with a targeted double-strand break (DSB) at the target locus in the genome. Coupling an ssODN donor with a CRISPR-Cas9-mediated DSB is one of the most streamlined approaches to introduce small changes. However, in many systems, this approach is inefficient and introduces imprecise repair at the genetic junctions. We herein report a technology that uses spatiotemporal localization of an ssODN with CRISPR-Cas9 to improve gene alteration. We show that by fusing an ssODN template to the trans-activating RNA (tracrRNA), we recover precise genetic alterations, with increased integration and precision in *vitro* and *in vivo*. Finally, we show that this technology can be used to enhance gene conversion with other gene editing tools such as transcription activator like effector nucleases.

Introduction

Targeted genomic alterations have revolutionized the field of molecular biology. Most recently, efforts have focused on CRISPR and cognate CRISPR-associated proteins (Cas), namely Cas9.[1–3] Cas effectors are directed to a region in the genome by a ~20 nt guide RNA and induce a targeted double-strand break (DSB).[3] In the absence of a repair template, the cell typically repairs the lesion by an un-templated repair pathway such as non-homologous end joining (NHEJ)[4] or alternative end joining (Alt-EJ).[5,6] In the presence of a repair template such as a single-stranded DNA (ssDNA) or a double-stranded DNA (dsDNA) template, precise repair is triggered that is directed by regions of homology on the donor.[7]

Repair with a dsDNA donor is relatively inefficient in most cell types.[8] Alternatively, repair via an ssDNA donor is efficient in multiple systems[8–10] and has been demonstrated to be efficient in primary cell types such as T cells for the generation of chimeric antigen receptor T cells[11] as well as induced pluripotent stem cells (iPSCs).[12] Studies have demonstrated that ssODNs are sufficient for inserting small (<50 bp) changes into the genome at appreciable rates.[13] Whereas dsDNA-mediated gene replacement uses homologies of ~0.5–1 kbp, ssDNA-mediated gene replacement often proceeds using shorter homologies.[14] For example, the length of flanking homologies has been shown to be less important with smaller cargos.[14,15]

Rates of homology-directed repair (HDR) with Cas9-mediated DSBs and an ssODN in zebrafish are typically modest,[16,17] with imprecise sequence changes regularly introduced at the genetic junctions.[18] Imprecision at the insertion junctions has been explained partly by the integration of fragments of the ssODN template.[19] Though ssODN-mediated changes are sufficient for some applications, the low efficiency and imprecision can make this difficult to deploy in highly precise applications.

Recent work has shown that spatiotemporal localization of an ssODN via covalent linkage to Cas9 increases rates of HDR.[20,21] However, these approaches require protein–nucleic acid engineering and can be complex to adopt. The observations using a protein–nucleic acid

[1]Department of Biochemistry and Molecular Biology, [2]Department of Clinical and Translational Sciences, [3]Mayo Clinic Graduate School of Biomedical Sciences, Virology and Gene Therapy Track, and [4]Mayo Clinic Graduate School of Biomedical Sciences, Biomedical Engineering and Physiology Track, Mayo Clinic, Rochester, Minnesota, USA.

*Address correspondence to: Stephen C. Ekker, PhD, Department of Biochemistry and Molecular Biology, Mayo Clinic, 200 1st Street SW, Rochester, MN 55905, USA, Email: Ekker.Stephen@mayo.edu

fusion suggest that improving spatiotemporal localization of the repair template to the site of the DSB increases rates of HDR.

Even when targeted, DNA DSBs are still a threat to genomic integrity. Unexpected alterations such as small insertions and deletions (indels) and chromosomal rearrangements are common genetic byproducts. Due to the potentially detrimental consequences, methods have been developed that preclude a targeted DSB coupled with a repair template, including base editing (BE)[22,23] and prime editing (PE).[24] Though these technologies do not require DSB-triggered HDR, they are not without drawbacks. Even with several iterations of the BE system, the editing window remains relatively large and renders precision applications difficult. Additionally, prime editing requires several large and potentially toxic or immunogenic components and relies on delivery and activity of a viral reverse transcriptase.

We herein report a methodology that is backwards compatible with CRISPR-Cas9 that uses spatiotemporal components of CRISPR-Cas9 and minimal homologies sufficient for small DNA modifications. We demonstrate that covalent fusion of an ssDNA repair template to the tracrRNA, deliverable as CRISPR-Cas9 RNP, results in precise gene conversion with as little as 10 nt of homology. We demonstrate that our approach, which we term Donorguide, is amenable to both *in vitro* and *in vivo* applications. Additionally, we find that Donorguide can enhance the activity of other gene editing tools such as transcription activator like effector nucleases (TALENs) to increase HDR.

Methods

Cell culture

HEK293T cells were obtained from ATCC (CRL-3216). Cells were maintained in Dulbecco's modified Eagle's medium (DMEM; Gibco #11995-040) supplemented with 10% fetal bovine serum (Gibco #26140079) and 1% penicillin/streptomycin (Gibco #15140-122).

In vitro *Donorguide RNP preparation*

crRNAs (Supplementary Table S1) were ordered from Integrated DNA Technologies and suspended at a concentration of 200 μM in 1×TE. The chimeric tracrRNAs were ordered from IDT as RNA ultramers (Supplementary Table S1) and suspended at a concentration of 200 μM in 1×TE. To assemble the Donorguide for *in vitro* studies, 3 μL of 200 μM crRNA was combined with 3 μL of 200 μM chimeric tracrRNA and heated to 95°C for 5 min and immediately removed to cool on the bench top to room temperature (RT) for 10–20 min.

Five microliters of the 100 μM crRNA:tracrRNA was added to a new nuclease-free polymerase chain reaction (PCR) tube. Four microliters of Alt-R Cas9 Nuclease 3NLS (62 μM stock; IDT cat. #1074181 1074182) was added to bring to the final volume to 9 μL, and this was incubated at RT for 20–30 min to form the RNP complex.

Transfections

For Donorguide HEK293T electroporations, 9 μL of Donorguide RNP complex (see above) was diluted with 16 μL in EP buffer (Etta Biotech Co.) to make a final volume of 25 μL. For ssODN HEK293T electroporations, 5 μL of 100 μM ssODN was added to 9 μL of the CRISPR-Cas9 RNP and diluted to 25 μL with EP. Diluted Donorguide or CRISPR-Cas9 RNP was added to 300 μL HEK293T cells at a concentration of 20E6 cells/mL in EP buffer and mixed thoroughly. Then, 105 μL of the HEK293T cell+ RNP was added to triplicate cuvettes.

For TALEN dCas9 Donorguide electroporations, 9 μL of dCas9 Donorguide RNP or 5 μL of 100 μM ssODN with 4 μL phosphate-buffered saline (PBS) was brought to 25 μL with EP buffer. Donorguide RNP complex or ssODN mix was added to 300 μL HEK293T cells in EP buffer at a concentration of 20E6 cells/mL and mixed thoroughly. Then, 107 μL of the HEK293T cell+ Donorguide cocktail was equally distributed to three Eppendorf tubes. Two-and-a-half micrograms of each of the TALEN arm plasmids were added to each tube and then transferred to an electroporation cuvette.

HEK293T cells were electroporated with Etta H1 electroporator (Etta Biotech Co.) with the following parameters: 200 V, 784 ms interval, six pulses, and 1,000 μs duration. Cells were then transferred to a six-well tissue cell culture plate at a density of about 1.5E6 cells/mL in complete DMEM.

HEK239T cell DNA isolation and PCR amplification

DNA from whole-cell populations was purified using the Qiagen DNeasy Blood and Tissue Kit (Qiagen; 69504). PCR amplification was conducted with Platinum SuperFi DNA Polymerase (Thermo Fisher Scientific; 12351010) or Q5® High-Fidelity 2×Master Mix (New England Biolabs; M0492S) and purified with the Qiagen QIAquick PCR Purification Kit (Qiagen; 28104).

GENEWIZ AmpliconEZ: DNA library preparation and Illumina sequencing

PCR products were obtained and purified as mentioned above. Illumina partial adapters (forward sequencing read: 5′-ACA CTC TTT CCC TAC ACG ACG CTC TTC CGA TCT-3′; reverse sequencing read: 5′-GAC TGG AGT TCA GAC GTG TGC TCT TCC GAT CT-3′) were added to the 5′ end of sequencing primers. DNA

library preparations, sequencing reactions, and initial bioinformatics analyses were conducted at GENEWIZ, Inc. DNA library preparation, clustering, and sequencing reagents were used throughout the process using the NEBNext Ultra DNA Library Prep Kit, following the manufacturer's recommendations (Illumina).

End-repaired adapters were ligated after adenylation of the 3′ ends followed by enrichment by limited cycle PCR. DNA libraries were validated on the Agilent TapeStation, quantified using the Qubit 2.0 Fluorometer (Invitrogen), and multiplexed in equal molar mass. The pooled DNA libraries were loaded on the Illumina instrument according to the manufacturer's instructions. The samples were sequenced using a 2×250 paired-end (PE) configuration. Image analysis and base calling were conducted by the Illumina Control Software on the Illumina instrument.

Next-generation sequence analysis

The .fasta files obtained from GENEWIZ AmpliconEZ were analyzed using CasAnalyzer[25] to determine indel efficiency and overall HDR events. The output from CasAnalyzer was further analyzed utilizing NGS Analyzer, an in-house script developed to quantify precise and imprecise HDR events rapidly. NGS Analyzer is hosted at https://github.com/srcastillo/Sequencing under a GNU General Public License v3.0.

TALEN design and assembly

A 15-14-15 TALEN design strategy was employed for this assay. Two 15-mer repeat variable di-residue (RVD) TALENs with a 14 bp spacer were designed to target *EGFP* (Supplementary Table S1) and generated using the FusX assembly system.[26] The RVDs utilized were HD = C, NN = G, NI = A, and NG = T.

Zebrafish husbandry

Wild-type (WT) Mayo Recessive Free (MRF) zebrafish (*Danio rerio*) were maintained in the Mayo Clinic Zebrafish Core Facility in accordance with standard practices[27] and guidelines from the Institutional Animal Care and Use Committee (A34513-13-R16, A8815-15). MRF fish are WT fish stock that have been maintained through diverse outbreeding schemes to ensure genetic diversity and have undergone screening processes each generation to ensure that the lines do not carry recessive phenotypes.

Adult zebrafish are kept in 9 L (25–30 fish) or 3 L (10–15 fish) housing tanks at 28.5°C with a light/dark cycle of 14/10 hours. Adult fish pair breeding was set up a day before microinjections, and dividers were removed on the morning of the injection day. After microinjections, the embryos were transferred to Petri dishes (100 mm) in E2 media (1×; 15 mM NaCl, 0.5 mM KCl, 1 mM $MgSO_4$, 150 μM KH_2PO_4, 50 μM Na_2HPO_4, 1 mM $CaCl_2$, 0.7 mM $NaHCO_3$) and maintained in an incubator at 28.5°C.

Sexes are not determined in larval fish (2–5 days post fertilization [dpf]) in this study, and thus potential differences based on sex are not assessed.

DNA oligonucleotide preparation

All ssODNs used in this study were purchased from IDT. Stock was prepared at 100 μM in 1×TE, and working stock was prepared at 20 μM to be used for microinjection or left at 100 μM for *in vitro* studies.

crRNA, tracrRNA, Donorguide, and SpCas9 preparation for zebrafish microinjection

crRNA, tracrRNA, Donorguide, and SpCas9 were custom ordered from IDT. Stock was prepared at 20 μM in duplex buffer (IDT; cat. #11-05-01-03; 30 mM HEPES, pH 7.5, 200 mM potassium acetate) for crRNA, tracrRNA, and Donorguide. At the 20 μM concentration, crRNA is at 233.9 pg/nL (protospacer length 20 nt), and tracrRNA is at 432.7 pg/nL. SpCas9 stock was prepared at 23 μM (3.73 ng/nL) in PBS (1×).

Microinjection

One-cell stage fertilized zebrafish embryos were harvested and aligned on an agarose plate in E2 media. Three microliters of injection solution was loaded into an injection needle as described previously.[28] A 2 nL of injection solution was delivered into the cell interface layer of the embryo. This injection (2 nL) delivered crRNA:tracrRNA (or Donorguide):SpCas9 complex at approximately 4.52 fmol (52.9 pg):4.52 fmol (97.8 pg):4.52 fmol (733.1 pg) and ssODN (when needed) at 4 fmol. Injected embryos were transferred to a new Petri dish and kept in an incubator at 28.5°C. Dead and nonviable embryos were counted and removed the next day (1 dpf).

Zebrafish experimental replicates

All experiments involving zebrafish microinjection were carried out in three independent experiments. Each experiment utilized a mixed populations of embryos obtained from multiple clutches. Each experiment was ideally conducted on different days. If two experiments were performed on a day, all reagents were prepared from different stock preparations.

Zebrafish genomic DNA extraction

Typically, 40 embryos were individually collected in 36 μL of NaOH (50 mM) 1–2 dpf (if morphological phenotyping was not necessary) and 4–5 dpf (if morphology was assessed). Each embryo was placed in 36 μL 50 mM

NaOH and heated at 95°C for 15 min with regular vortexing. To stabilize NaOH, 4 μL of Tris-HCl (1 mM, pH 8) was added. Eight embryos were pooled into a sample (a biological replicate) by taking 2 μL from each embryo (eight fish per sample), and a 1:3 dilution was made by adding 48 μL of distilled water.

Statistical analyses

We compared between conditions using an unpaired *t*-test and used the Holm–Sidak method to correct for multiple comparisons. Differences between groups were considered significant at a *p*-value of <0.05. Statistical analyses were performed with GraphPad Prism v8.4 (GraphPad Software, Inc., San Diego, CA).

Results

Donorguide SpCas9 introduces precise insertions more efficiently than ssODN donors

To assess the feasibility of covalently tethering a DNA template to the 3′ of a tracrRNA to induce precise genetic edits, we employed HEK 293T cells for their ease of transfection (Fig. 1). We previously identified an active *Streptococcus pyogenes* Cas9 (SpCas9) CRISPR RNA (crRNA):tracrRNA reagent targeting a locus in the safe harbor region *AAVS1* (Supplementary Fig. S1).[29,30] Due to synthetic RNA synthesis length limits, we used separate CRISPR RNA (crRNA) and tracrRNA instead of single-guide RNA.[31] The tracrRNA was synthesized with a DNA repair template fused to the 3′ end containing 12 nt of homology flanking a 2 nt insertion (Fig. 2A) generating a chimeric RNA:DNA hybrid.

The chimeric tracrRNA was annealed with an SpCas9 crRNA to form what we term the Donorguide and combined with SpCas9 recombinant protein to form the RNP complex. HEK293T cells were electroporated with Donorguide RNP and screened for genetic insertions by next-generation sequencing (NGS; Fig. 1). We found that the Donorguide SpCas9 RNP introduced the precise 2 nt insertion at an efficiency of 1.1 ± 0.50% (mean ± standard deviation; Fig. 2B). In addition, we found that

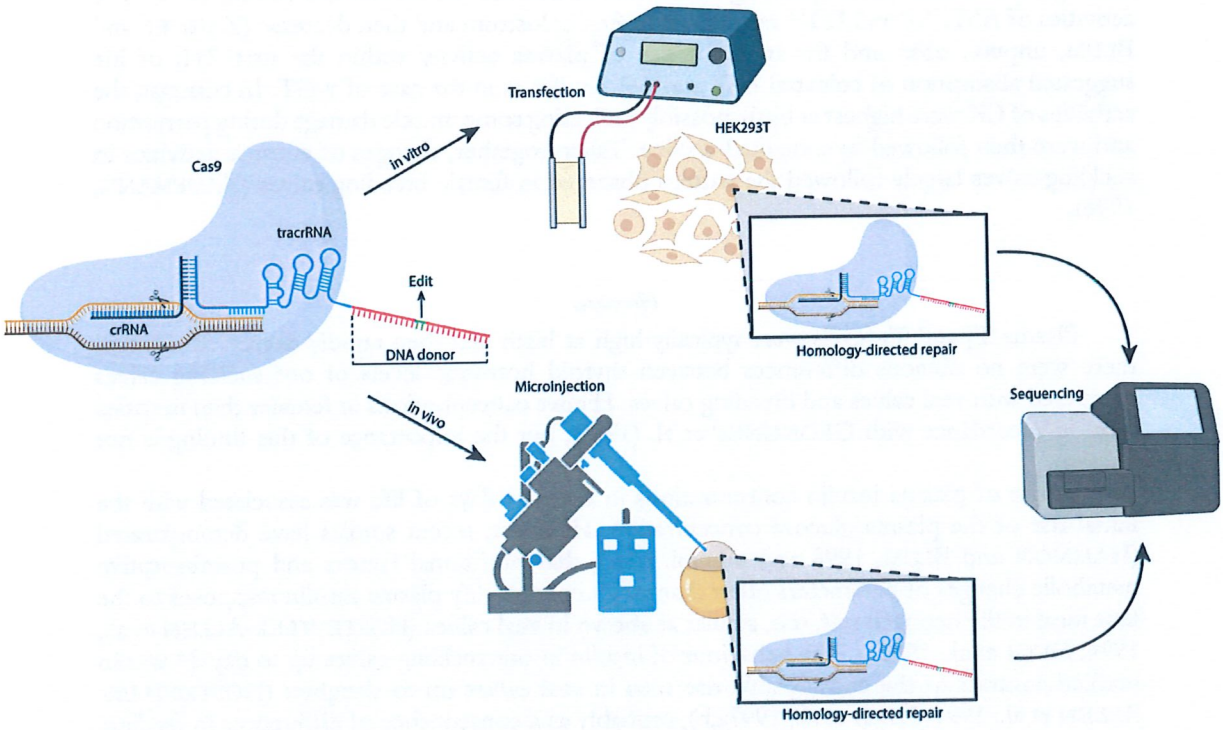

FIG. 1. Donorguide composition and experimental workflow. Left: Donorguide consists of a canonical CRISPR RNA (crRNA) and trans-activating crRNA (tracrRNA) that is fused to a DNA repair template. Top: *In vitro* experiments were carried out by electroporating Donorguide RNP complexes into cells and culturing before DNA isolation for next-generation sequencing (NGS) analyses. Bottom: *In vivo* experiments were carried out by microinjecting single-cell zebrafish embryos with Donorguide RNP complexes and collecting larvae on 1 or 3 days post fertilization (dpf) for NGS. Color images are available online.

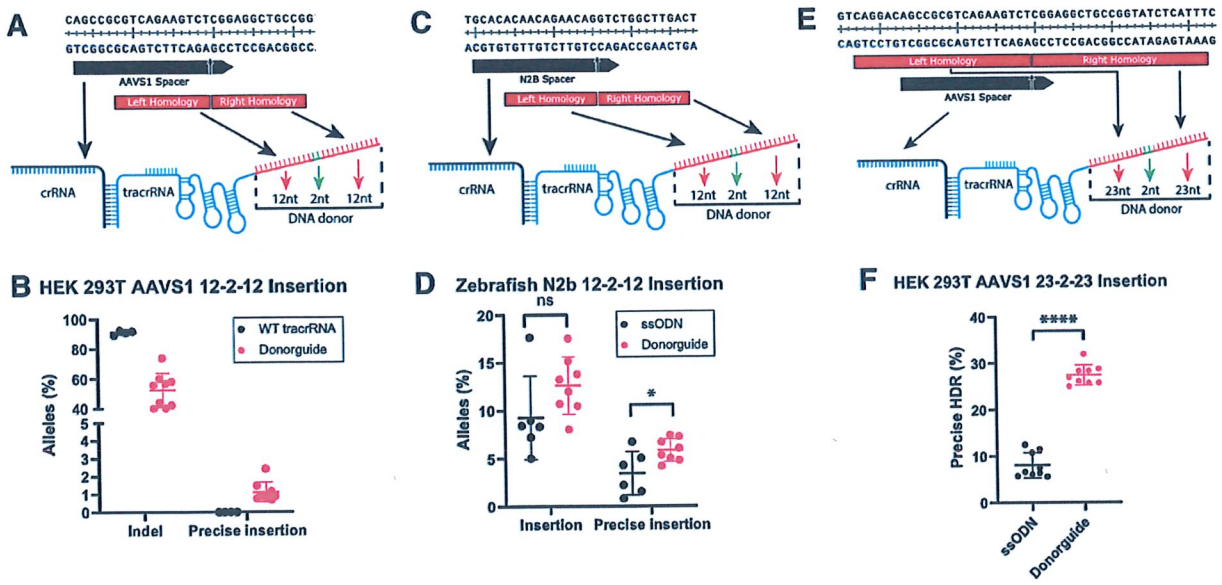

FIG. 2. CRISPR Donorguide catalyzes precise insertions *in vitro* and *in vivo*. HEK293T cells were transfected, and zebrafish one-cell stage embryos were injected with either CRISPR Donorguide:SpCas9 RNP complex or crRNA:tracrRNA:SpCas9 RNP complex with a single-stranded oligo deoxynucleotide (ssODN). **(A)** *AAVS1* CRISPR-Cas9 target site and corresponding Donorguide design. A 2 nt insert was introduced flanked by 12 nt of homology to the genomic target site. **(B)** Quantification of CRISPR Donorguide knock-in in HEK293T cells. Homology-directed repair was quantified by CasAnalyzer[25] and then filtered by NGS Analyzer to call precise insertion events. **(C)** The CRISPR-Cas9 target site and corresponding CRISPR Donorguide design in N2B exon of *ttn.2*. A 2 nt insert was introduced flanked by 12 nt of homology to the genomic target site. **(D)** Quantification of CRISPR Donorguide knock-in in zebrafish. For all *in vivo* NGS experiments, the NGS data of DNA from injected zebrafish were analyzed by CasAnalyzer and further filtered by NGS Analyzer to call precise insertion events. **(E)** A 2 nt insertion flanked by 23 nt of homology was introduced. **(F)** Quantification of CRISPR Donorguide at *AAVS1*. For all *in vitro* NGS experiments, the NGS data of cells were analyzed by CasAnalyzer and further filtered by NGS Analyzer to call precise insertion events. Individual values of three independent experiments. Color images are available online.

Donorguide (52±11%) introduced indel mutations at markedly lower rates than a tracrRNA (91±2%). These data suggested that the Donorguide methodology is a viable approach to introduce precise small molecular changes *in vitro*, albeit at modest rates.

Encouraged by our *in vitro* results, we sought to see whether Donorguide likewise functions *in vivo*. We chose zebrafish (*Danio rerio*) due to their high fecundity, amenability to microinjection, and ease of genotyping (Fig. 1). Single-cell embryos were injected with SpCas9 RNP with a crRNA targeting the N2B exon in the *titin* gene locus that we have previously shown to be highly active[6] (Fig. 2C), along with an ssODN donor providing a 2 nt insertion or CRISPR Donorguide containing the same 2 nt insertion. Injected animals were incubated for 72 h before having their genomic DNA isolated, PCR amplified, and submitted for NGS (Fig. 1).

We found that using Donorguide, compared to SpCas9 and an ssODN donor, results in a similar rate of overall HDR events (9.3±4.3% for ssODN and 13±3% for Donorguide) composed of both precise and imprecise insertion events (Fig. 2D). However, the genetic alterations induced by Donorguide (5.9±1.2%) resulted in a higher rate of precise insertions when compared to an ssODN donor (3.4±2.7%; Fig. 2D) and Donorguide insertions transmit to the offspring (Supplementary Fig. S4).[32]

Seeking to replicate our appreciable *in vivo* knock-in results, we sought to determine whether the size of the homology arms accounted for the modest rates of HDR with CRISPR Donorguide *in vitro* (Fig. 2B). To address this, we increased the homology arm length to 23 nt for both CRISPR Donorguide and its requisite ssODN designed to introduce a 2 nt insertion at *AAVS1* (Fig. 2E).

The 23-2-23 Donorguide or SpCas9 and ssODN were electroporated into HEK293T cells and analyzed for HDR by NGS. We found that using larger homologies flanking the insertion resulted in precise HDR rates of 27 ± 2.2% with CRISPR Donorguide compared to Cas9 and an ssODN donor that resulted in 8.1 ± 2.7% precise HDR (Fig. 2F). Taken together, these data suggest that CRISPR Donorguide can introduce HDR at appreciable rates and outperform a comparable ssODN DNA donor.

Donorguide SpCas9 introduces precise substitutions more efficiently than ssODN donors

We next set out to assess whether Donorguide could introduce precise genetic substitutions. To this end, we employed an established EGFP-BFP reporter system[33] to measure genetic substitution fluorometrically. *EGFP* contains 2 aa in its chromophore domain, Thr65 and Tyr66, which when mutated to Ser65 and His66 converts to *BFP*, which can be recorded by flow cytometry (Fig. 3A).[33] HEK293T cells were transfected with an *EGFP*-expressing plasmid that is flanked by Tol2 inverted terminal repeats as well as a plasmid encoding Tol2 transposase (Supplementary Table S1). Cells were passaged several times and were FACS sorted for the brightest *EGFP*-expressing cells to establish the HEK-EGFP reporter cell line (Supplementary Fig. S2).

HEK-EGFP cells were transfected with Donorguide or SpCas9 with an ssODN containing the EGFP-BFP substitutions flanked by 10 nt of homology (Fig. 3A and B). Cells were incubated at 37°C for 72 h and measured for *BFP* expression by flow cytometry. Compared to SpCas9 and an ssODN (0.49 ± 0.11% BFP+), Donorguide converted *EGFP* to *BFP* at a significantly greater rate (1.7 ± 0.48% BFP+) as measured by flow cytometry (Fig. 3C and D) and NGS (Supplementary Fig. S3). These results suggest that when compared to a free ssODN of similar size, CRISPR Donorguide results in a quantitative improvement of HDR induction *in vitro*.

To assess whether conversion of EGFP-BFP observed in our HEK-GFP reporter can also be deployed *in vivo*, we employed a previously established transgenic zebrafish line that has an *EGFP* reporter stably integrated into its genome[34] (Fig. 3E) that transmits at a Mendelian ratio. Single-cell embryos were injected with either SpCas9 and an ssODN or Donorguide encoding the EGFP-BFP transition. Injected animals were pooled, had their DNA isolated, were barcoded, and were submitted for NGS. We found that CRISPR Donorguide (1.7 ± 1.3%) results in more precise insertion events compared to an ssODN of a similar size (0.13 ± 0.17%; Fig. 3F). These results suggest that CRISPR Donorguide functions cross-model to enhance gene substitution relative to an ssODN.

Donorguide SpCas9 introduces precise deletions more efficiently than ssODN donors

Small insertions comprise about 3% of known human pathogenic genetic variants,[24] and being able to correct these aberrant sequences to restore the WT gene is highly sought after. Targeting insertion regions with CRISPR-Cas9 to resolve the lesion can result in additional loss of function alleles as a result of inadvertent activation of NHEJ or Alt-EJ. Therefore, precise deletions are required to address such conditions. To this end, we set out to determine if Donorguide could introduce precise deletions at higher rates than a comparable ssODN. To assess precise deletion, we developed a reporter cell line such that unperturbed cells will be EGFP+, but if a precise deletion of the stop codon is introduced the cells will be EGFP+/mRFP+ (Fig. 4A). HEK EGFP cells were transfected with either SpCas9 and an ssODN encoding the 3 nt stop codon deletion or with CRISPR Donorguide, incubated for 72 h, and assessed for precise deletion by NGS. We found that CRISPR Donorguide introduced the precise deletion at nearly the same rate as an ssODN (11 ± 3.5% ssODN and 10 ± 4.0% Donorguide). However, in agreement with previous observations (Fig. 2B), we note that Donorguide resulted in a significantly decreased amount of overall indel mutations compared to SpCas9 (89 ± 10% ssODN and 41 ± 15% Donorguide).

Accordingly, Donorguide resulted in a significantly greater percentage of precise deletion alleles, defined as the number of desired alterations/overall indel mutations (25 ± 1.7% Donorguide and 13 ± 2.9% ssODN; Fig. 4B). These results suggest that CRISPR Donorguide can introduce a precise deletion at a comparable rate to an ssODN, but the overall fraction of desired alleles is significantly greater in the mutant allele population.

Modeling clinically relevant mutations in animal models is a top priority in the field of precision genomics. Therefore, we sought to determine if we could employ CRISPR Donorguide to model small molecular changes in a clinically relevant gene. To this end, we chose the gene *nr3c1*, which is a cognate cortisol receptor and encodes a glucocorticoid receptor that mediates hypothalamic–pituitary–inter-renal axis activation in zebrafish and is used to model the human acute stress response.[35] We targeted *nr3c1* with SpCas9 and provided an ssODN or Donorguide consisting of 12 nt of homology designed to delete 8 bp (Fig. 4C).

As noted in the *in vitro* deletion study, we found comparable rates of overall precise deletion between ssODN

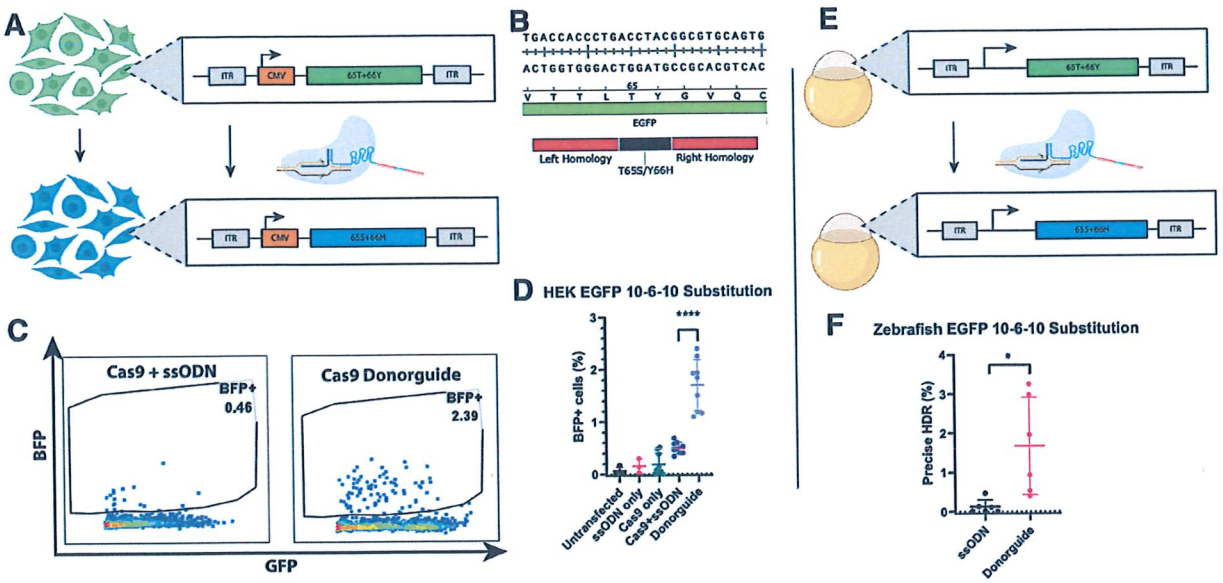

FIG. 3. CRISPR Donorguide catalyzes precise substitutions *in vitro* and *in vivo*. **(A)** Schematic diagram of EGFP-BFP conversion cell reporter. HEK GFP cells were made by Tol2 transposition followed by FACS sorting. HEK EGFP cells were electroporated with CRISPR Donorguide or an ssODN encoding the 2 aa substitution flanked by 10 nt of homology. Transfected HEK GFP cells were analyzed for BFP expression by flow cytometry 72 h post transfection. **(B)** Donorguide and ssODN design containing the 2 aa substitution flanked by 10 nt of homology. **(C)** Representative flow cytometry data of HEK EGFP cells transfected with either SpCas9 and an ssODN encoding the EGFP-BFP substitution or with CRISPR Donorguide carrying the EGFP-BFP mutation. **(D)** Quantification of BFP+ cells transfected with CRISPR Donorguide or SpCas9 and an ssODN donor by flow cytometry. **(E)** Schematic diagram of EGFP-BFP conversion in zebrafish. Transgenic zebrafish with EGFP integrated into the genome by Tol2 transposition were injected at the single-cell stage with either CRISPR Donorguide or SpCas9 and an ssODN encoding the EGFP-BFP substitution. **(F)** Quantification of EGFP-BFP substitution *in vivo*. Individual values of three independent experiments. Color images are available online.

(0.61 ± 0.29%) and Donorguide (0.33 ± 0.21%) when considering all alleles. In agreement with our previous studies with SpCas9 and an ssODN, SpCas9 resulted in significantly more indels (88 ± 8.4%) compared to Donorguide (9.8 ± 5.3%). Accordingly, when considering the proportion of desired alleles in the mutant allele population, Donorguide resulted in a significantly greater (3.4 ± 1.4%) percentage of mutant alleles when compared to an ssODN (0.96 ± 0.31%; Fig. 4D). These results suggest that although Donorguide may introduce a similar overall number of precise deletions compared to an ssODN, Donorguide-mediated deletions comprise a greater proportion of the mutant allele population.

Increased rates of precision editing with Donorguide enable phenotype screening in animals

As we observed that Donorguide generated a greater proportion of desired deletions in mutant alleles, we tested whether we could leverage this phenomenon to streamline the generation of animal models. We developed an assay to remove WT alleles effectively from the population while simultaneously interrogating whether the remaining mutant alleles were generated by random indels or precise HDR.

To this end, we targeted the tyrosinase (*tyr*) gene in zebrafish, which is required for converting tyrosine into the pigment melanin that confers skin color.[36] We inserted a 6 nt *Avr*II restriction site with either an ssODN or Donorguide into the *tyr* locus (Fig. 5A). If precisely inserted, the cargo will generate an in-frame stop codon and should lead to the development of zebrafish with pigmentation phenotypes (Fig. 5B). Zebrafish were injected, and the resulting pigmentation mutants segregated and pooled. Their genomic DNA was isolated, PCR amplified, and subsequently submitted for NGS.

Interestingly, while Cas9 and the ssODN generated a strong albino-like phenotype (Fig. 5D), we observed only apparent WT zebrafish in the Donorguide condition

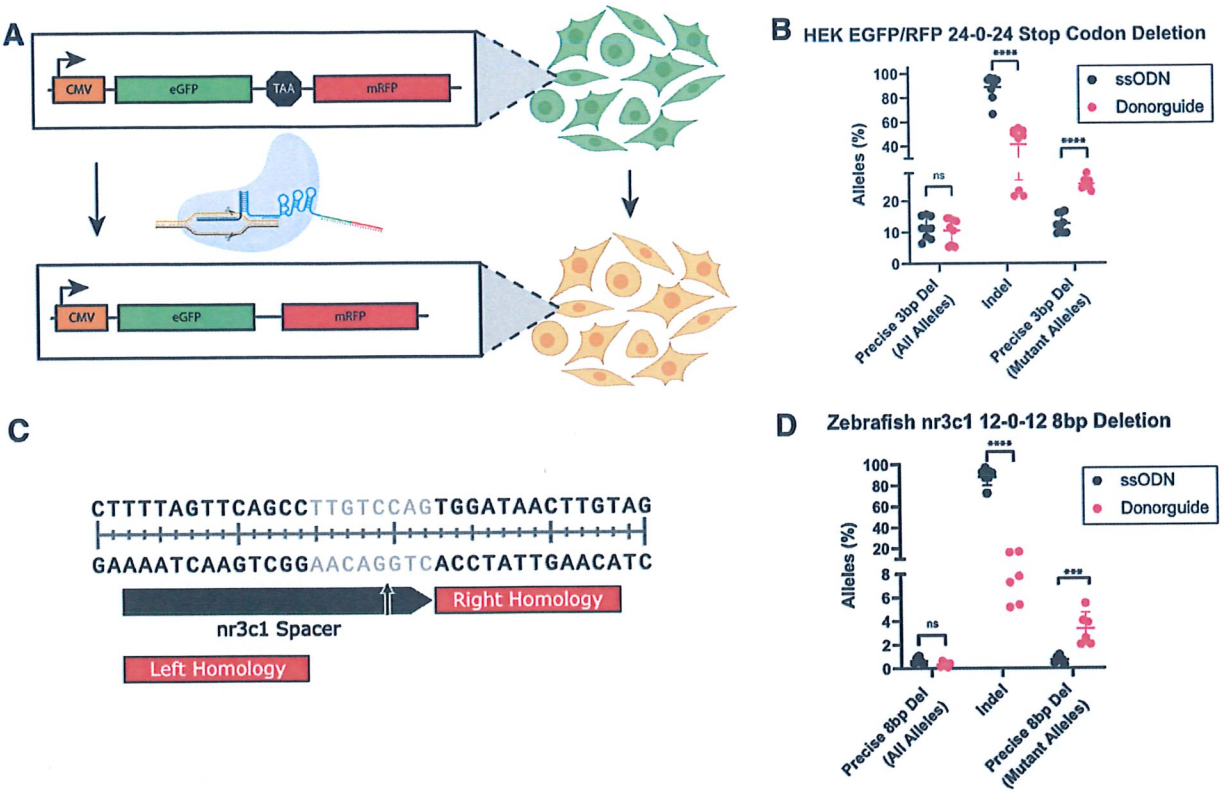

FIG. 4. CRISPR Donorguide introduces a greater proportion of precise deletions. **(A)** Schematic representation of EGFP/mRFP reporter cell line. EGFP and mRFP separated by a stop codon were introduced into HEK293T cells by Tol2 transposon and sorted for the highest expressing EGFP+ cells. When a donor is introduced that removes the stop codon, HEK EGFP cells become EGFP/mRFP double positive. **(B)** Quantification of precise deletion in HEK EGFP. HEK EGFP cells transfected with CRISPR Donorguide or an ssODN encoding the 3 nt deletion were analyzed for the precise 3 bp deletion 72 h post transfection by NGS. **(C)** *nr3c1* CRISPR Cas9 target site and corresponding CRISPR Donorguide design. Gray base pairs correspond to the region being deleted. The deletion was introduced with a donor consisting of 12 nt flanking the target nucleotides. **(D)** Quantification of precise deletion in zebrafish at *nr3c1*. Individual values of three independent experiments. Color images are available online.

(Fig. 5E). This observation was supported by sequencing analysis that showed the Cas9- and ssODN-injected albino zebrafish consisted of almost entirely (97±0.95%) indel alleles (Supplementary Fig. S5). The Donorguide-injected animals did not have a visible pigmentation phenotype (and were therefore randomly pooled without segregation based on phenotype) and had only 24±2.8% indel alleles, which was likely not sufficient to produce an apparent pigmentation phenotype (Supplementary Fig. S5).

We found that the DNA portion of the *tyr* chimeric tracrRNA was designed complementary to the crRNA target strand. We reasoned that the DNA region of the chimeric tracrRNA and the crRNA were aberrantly annealing during Donorguide assembly and preventing the formation of the crRNA:Donorguide duplex. We then designed the *tyr* chimeric tracrRNA DNA region to be of the same strand as the crRNA target strand, and therefore prevent aberrant base pairing. Upon switching the strandedness of the DNA donor portion, we observed strong albino phenotypes and requisite nuclease activity using the same strand Donorguide (Fig. 5F and Supplementary Fig. S5) at approximately the same rates as the Cas9- and ssODN-injected conditions (Supplementary Fig. S6).

We note that when comparing the ssODN and Donorguide of the same strand, Donorguide resulted in significantly more overall HDR events (23±6.5%) than Cas9 and an ssODN did (5.5±3.1%; Fig. 5G). Additionally, we found Donorguide introduced significantly more precise HDR events (11±6.1%) compared to a canonical

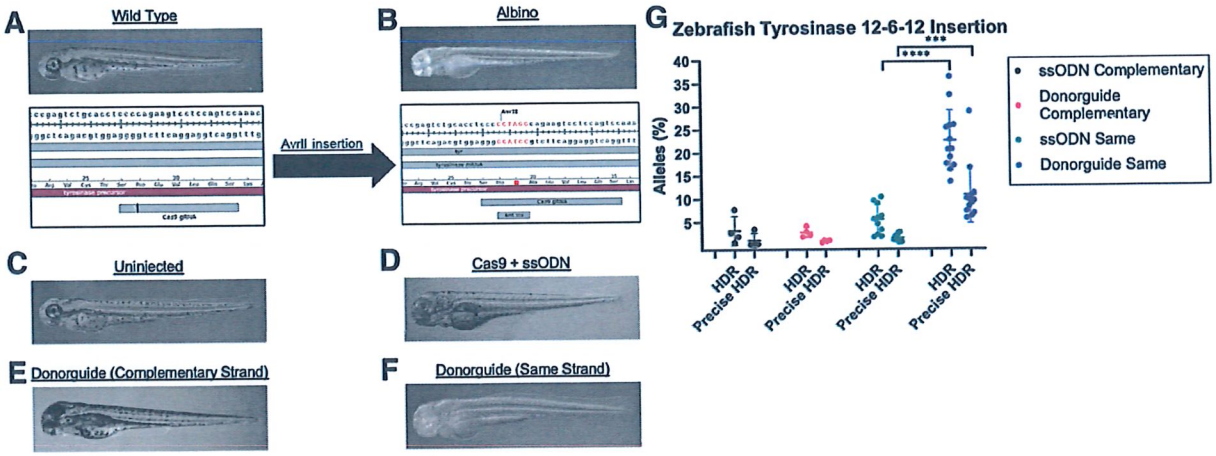

FIG. 5. CRISPR Donorguide increases the rate of precise sequence changes found in gene edited animals screened to identify a desired alteration. **(A)** Schematic representation of the *tyr* locus and Cas9 crRNA target site. The tyrosinase gene is involved in melanin biosynthesis and drives spotted pigmentation patterns in larval zebrafish and horizontal striped pigmentations in adult zebrafish. WT *tyr* zebrafish show pigmentation patterns in the body and eyes. **(B)** Schematic representation of the *tyr* locus with the *Avr*II site inserted and generating a premature stop codon. The subsequent nonsense mutation results in zebrafish lacking body and lens pigmentation. **(C)–(F)** Representative images of zebrafish targeted at the *tyr* locus with either an ssODN or Donorguide. **(G)** Quantification of albino-like mutant zebrafish injected with either ssODN or Donorguide inserting the *Avr*II site into the *tyr* locus. Individual values of three independent experiments. Color images are available online.

ssODN (1.5 ± 0.74%; Fig. 5G). These results suggest that when eliminating WT alleles by phenotypic screening, CRISPR Donorguide-mediated insertions at the *tyr* locus comprise approximately a quarter of the mutant allele population. Importantly, the HDR events that are introduced with Donorguide are significantly more precise than those from an ssODN.

Donorguide works in concert with other gene editing technologies

Even with the advent of CRISPR orthologs such as Cas12a[37] and enhanced CRISPR-Cas9 variants with decreased protospacer adjacent motif (PAM) stringency,[38] there is still a PAM and gRNA requirement that could preclude the utilization of CRISPR. This is particularly problematic when performing HDR, where it has been demonstrated that gene conversion is greatly enhanced when the genetic change is introduced proximally to the DSB.[12] TALENs have only a 5′ thymidine requirement, which can be overcome with mutant variants.[39,40] TALENs have been shown to function efficiently as gene editing tools *in vivo*[41] and *in vitro*[42] for both knockout and knock-in applications.[43]

To this end, we assessed whether Donorguide could enhance TALEN-mediated HDR. We designed TALENs targeting the *EGFP* chromophore domain using our previously established FusX assembly (Supplementary Table S1).[44] We designed a catalytically inactive Cas9 (dCas9) Donorguide containing the EGFP-BFP substitution with a crRNA targeting ~80 bp downstream of the TALEN target site to prevent steric interference between dCas9 and the TALENs. HEK EGFP cells were transfected with the EGFP TALENs and an ssODN or with dCas9 Donorguide containing the EGFP-BFP transition (Fig. 6A) and measured for BFP expression 72 h later by flow cytometry.

We found that TALENs with dCas9 Donorguide resulted in an approximate threefold increase in BFP+ cells compared to TALENs with an ssODN (7.6 ± 3.6% Donorguide and 1.3 ± 0.51% ssODN). Taken together, these data suggest that CRISPR Donorguide results in greater gene conversion than an ssODN and can be used in concert with non-CRISPR gene editing tools such as TALENs.

Discussion

We report a facile approach to introduce small genetic changes *in vitro* and *in vivo*. Our *in vitro* results suggest that Donorguide can be adapted to other cell types to study protein function, validate variants of uncertain significance, or generate isogenic cell lines. Additionally, Donorguide lends itself to the possibility of a gene

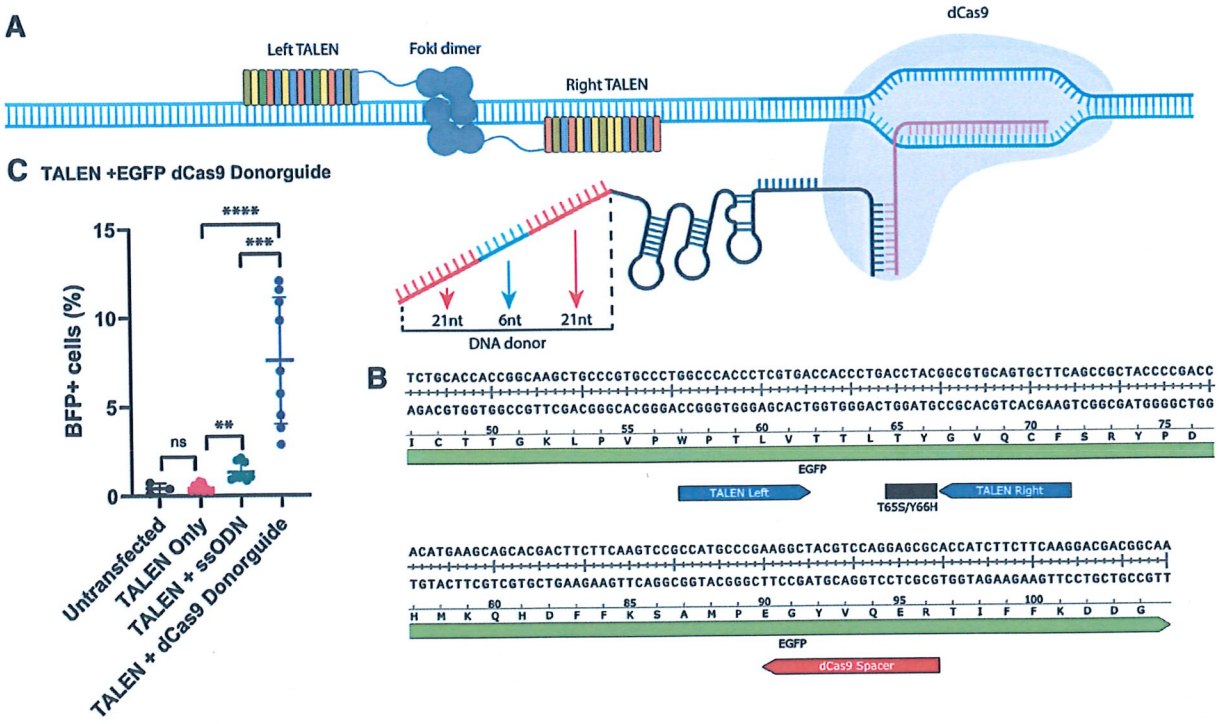

FIG. 6. CRISPR Donorguide functions synergistically with other gene editing tools *in vitro*. **(A)** Schematic diagram of transcription activator like effector nucleases (TALENs) targeting the EGFP chromophore domain coupled with dCas9 Donorguide. **(B)** dCas9 Donorguide targets the EGFP locus ~80 nt downstream of the TALEN target site and encodes the EGFP-BFP transition flanked by 21 nt of homology. **(C)** Quantification of EGFP-BFP conversion by flow cytometry. HEK GFP cells were transfected with TALENs and an ssODN encoding the EGFP-BFP transition or with TALENs and dCas9 Donorguide encoding the EGFP-BFP mutation. Transfected cells were measured for BFP expression 72 h post transfection by flow cytometry. Individual values of three independent experiments. Color images are available online.

therapy tool due to its decreased background indel mutations compared to SpCas9. We further show that this approach is amenable to editing *in vivo* using the zebrafish system. The success of Donorguide in zebrafish further suggests that this technology can be readily used to improve the generation of other *in vivo* models such as mice, rats, and larger animal models.

We found both a qualitative and quantitative improvement over standard ssODN methods using Donorguide *in vivo*. In zebrafish, our data suggest that for small genetic modifications it would be preferable to use the Donorguide to increase both the overall amount and precision of gene integration events. This feature enables researchers to make better animal models and should require less screening for allelic alterations. Imprecision of insertion events *in vivo* is well documented in the field[45–47] and has been partially explained by several phenomena, but a unifying explanation remains elusive. We observe genetic imprecision in zebrafish in agreement with previous reports using ssODN donors.[47]

We find that using Donorguide partially ameliorates some of the imprecision observed with ssODN donors. This could be explained, at least in part, by one of two factors. First, the nature of the DNA:RNA hybrid of the Donorguide could be less accessible to cellular nucleases and reduce the presence of donor fragments aberrantly integrating into the genomic lesion. Second, the Donorguide could be physically protected by the RNP complex likewise sparing it from cellular exonucleases that ssODNs are otherwise susceptible to similarly reducing the presence of donor DNA fragments.

There are limited reports of similar imprecision in mammalian systems. Accordingly, we observe little imprecision in our *in vitro* assays. We find that in our *in vitro* studies, the improvement of HDR with Donorguide compared to an ssODN is primarily an overall increase in desired mutant alleles without a significant change in precision of the integration events. We note one exception to this net increase of HDR events with Donorguide in our small deletion study. While we find

that while the net amount of precise deletion events is comparable between the ssODN and Donorguide, our approach results in a greater proportion of desired alterations in the pool of mutant alleles.

We recapitulated this increased mutant deletion allele proportion phenomena at the *nr3c1* locus in zebrafish. Our *nr3c1* observations, however, stood out for several reasons. First, the rate of precise deletions was surprisingly low for both ssODN and Donorguide. This low rate of HDR from both approaches suggests a locus-specific phenomenon contributing to poor HDR. Despite this, the trend of increased proportion of deletion alleles held consistent. Second, there was a sizable discrepancy of nearly a tenfold difference in indel induction between the ssODN and Donorguide at the *nr3c1* locus.

The relative decrease in Donorguide-mediated indels is consistent throughout this study. However, the difference was particularly profound at this locus. This dramatic decrease in indel induction suggests that there is likely some component of the DNA portion of the Donorguide that is preventing either the formation of the RNP or the nuclease activity of the RNP.

The presence of DNA fused to the 3′ end of the tracrRNA could disrupt the formation of the crRNA:tracrRNA duplex or Cas9 RNP complex. We calculated the change in entropy (ΔS) and Gibbs free energy (ΔG) by using the mfold web server (http://www.bioinfo.rpi.edu/applications/mfold) with default parameters except for prohibiting a string of consecutive bases from pairing in the first 20 bases (20 nt spacer). The ΔS and ΔG for crRNA:tracrRNA of each loci were predicted to be −650.65 cal/K/mol and −23 kcal/mol, respectively, upon duplexing. The magnitudes of ΔG for Donorguide (crRNA:chimeric tracrRNA) duplexes were considerably higher than the standard crRNA:tracrRNA complex (Supplementary Table S2).

The more negative ΔG values for the Donorguide duplexes suggest that the Donorguide complexes are generating more energetically favorable structures than the crRNA:tracrRNA duplex. Therefore, we hypothesize that the DNA portion of the Donorguide complex establishes stable local secondary structures at the 3′ end of the duplex. The stable Donorguide structure may alter the local topology around the classical terminal hairpins in the crRNA:tracrRNA duplex and result in inefficient RNP complex formation by disrupting protein–nucleic acid interactions.

In our *in vitro* studies, we note that increasing the lengths of homology flanking the insertion resulted in a marked increase in HDR events at *AAVS1*. We are currently generating these chimeric molecules from commercial manufacturers. While it is of interest to increase the length of the DNA portion of Donorguide systematically, chemical synthesis constraints are a limiting factor to broad access.

Current synthesis limits only allow for ~50 nt of DNA be added to the 3′ end of the tracrRNA, restricting the possibility of cargos and lengths of flanking homology. In-house synthesis of these chimeric molecules could afford the addition of larger homology arms flanking diverse cargos such as epitope tags or fluorescent reporter genes. Further study is needed to identify the ideal length that minimizes the formation of undesired structures and maximizes the use as a homologous repair template.

We leveraged the increased proportion of mutant alleles with Donorguide to streamline the generation of animal models by using the *tyr* locus in zebrafish. Screening for albino mutants showed significantly more insertion events in the Donorguide condition compared to ssODN. Donorguide can therefore be used to simplify the generation of animal models by decreasing the number of animals screened to find a desired mutant.

Being able to narrow down the editing outcomes to either a desired alteration or no editing at all may be desirable in the context of gene therapies such as for sickle cell disease (SCD) in which a point mutation causes the formation of sickled hemoglobin.[48] Though sickled hemoglobin is causal for the pathology of SCD, total loss of function via an inadvertent indel mutation would likely be more harmful than the original point mutant. In SCD and similar pathologies, Donorguide would therefore be a preferred method of correction in which the genetic outcome is more likely to be no editing at all or a precise alteration with less collateral genetic damage.

In this study, all the DNA portions of Donorguide are of the same strand as the crRNA. We find when using a crRNA complementary to the DNA portion of Donorguide, we observe poor editing *in vivo* (Fig. 5E and Supplementary Fig. S5). This phenomenon can likely be explained by the crRNA aberrantly base pairing with the DNA portion of the Donorguide and preventing either the formation of the Donorguide (crRNA:chimeric tracrRNA) duplex or with the formation of the Donorguide RNP complex.

We therefore developed several guidelines for Donorguide experiments: (1) identify a crRNA that is at least 50% active with SpCas9, as Donorguide tends to have decreased nuclease activity; (2) design the DNA repair template of the Donorguide to be of the same strand as the crRNA; and (3) for zebrafish, 12 nt of homology flanking a cargo of 2–6 nt should be a starting point for Donorguide design.

To our knowledge, the DNA portion of Donorguide follows the same rules as ssODN design, and therefore

an HDR design tool (IDT, horizon discovery, etc.) can be used to simplify the Donorguide design. We show that Donorguide results in either an overall increase of HDR events or an increased proportion of desired mutant alleles both *in vitro* and *in vivo* relative to a comparable ssODN. Divergent research applications could therefore leverage Donorguide for its desired editing outcomes. We likewise include design guidelines to deploy CRISPR Donorguide in diverse model systems for enhanced precision genome editing applications.

Conclusions

The ability to target the genome effectively for precise genetic alterations for gene therapy or to generate transgenic animal models is highly sought after. Here, we demonstrate precise genetic alterations in zebrafish and human cells with our newly developed CRISPR Donorguide. We show that Donorguide is a streamlined technology to introduce small genetic alterations both *in vitro and in vivo* with few custom reagents that are required for activity and is therefore a simple-to-adopt technology for most research labs.

In human cells, we show that Donorguide results in a greater amount of desired mutagenic events than a comparable ssODN. In zebrafish, we show CRISPR Donorguide introduces both qualitative and quantitative improvement over an ssODN donor by increasing both the overall amount and precision of HDR events. To assess the precision of HDR events, we developed NGS Analyzer to discern between precise and imprecise HDR events. Additionally, we show that Donorguide introduces less background indel mutations than standard CRISPR-Cas9.

Finally, we show that Donorguide can be used to enhance other gene editing technologies such as TALENs. The features of Donorguide described in this study suggest that with further optimization, Donorguide has the potential to be applied to clinical gene correction applications and enable the streamlined generation of transgenic animal models.

Acknowledgments

We thank the Mayo Clinic Zebrafish Facility staff for assisting with animal husbandry, and the Mayo Clinic Fluorescent Microscopy core for assistance with flow cytometry. We also thank Dr. Alex Abel for assistance with flow cytometry analysis. We additionally thank Drs. Maura McGrail and Jeff Essner for their constructive collaboration and advice. We further thank Dr. Matthew Schellenberg for his insightful conversation regarding the biophysics and stability of the chimeric molecules. We thank BioRender for providing templates for figure design.

Author Disclosure Statement

B.W.S. and S.C.E. have a financial interest in LEAH Laboratories and Mettaforge Therapeutics. S.C.E. and K.J.C. have a financial interest in LifEngine Biotechnologies and Recombinetics, Inc.

Funding Information

This work was supported by NIH grants OD020166, GM063904, and GM134732 (S.C.E. and K.J.C.), Mayo Foundation for Medical Education and Research (B.W.S., S.R.C., W.A.G., and G.M.G.), the Mayo Clinic Center for Regenerative Medicine and Michael S. and Mary Sue Shannon Foundation (B.W.S.), and the Harry C. and Debra A. Stonecipher Predoctoral Fellowship (S.R.C.).

Supplementary Material

Supplementary Table S1
Supplementary Table S2
Supplementary Figure S1
Supplementary Figure S2
Supplementary Figure S3
Supplementary Figure S4
Supplementary Figure S5
Supplementary Figure S6

References

1. Doudna JA, Charpentier E. The new frontier of genome engineering with CRISPR-Cas9. *Science* 2014;346:1258096. DOI: 10.1126/science.1258096.
2. Jinek M, Chylinski K, Fonfara I, et al. A programmable dual-RNA–guided DNA endonuclease in adaptive bacterial immunity. *Science* 2012;337:816–821. DOI: 10.1126/science.1225829.
3. Ran FA, Hsu PD, Wright J, et al. Genome engineering using the CRISPR-Cas9 system. *Nat Protoc* 2013;8:2281–2308. DOI: 10.1038/nprot.2013.143.
4. Mao Z, Bozzella M, Seluanov A, et al. Comparison of nonhomologous end joining and homologous recombination in human cells. *DNA Repair* 2008;7:1765–1771. DOI: 10.1016/j.dnarep.2008.06.018.
5. Bae S, Kweon J, Kim HS, et al. Microhomology-based choice of Cas9 nuclease target sites. *Nat Methods* 2014;11:705–706. DOI: 10.1038/nmeth.3015.
6. Ata H, Ekstrom TL, Martínez-Gálvez G, et al. Robust activation of microhomology-mediated end joining for precision gene editing applications. *PLoS Genet* 2018;14:e1007652. DOI: 10.1371/journal.pgen.1007652.
7. Richardson CD, Kazane KR, Feng SJ, et al. CRISPR-Cas9 genome editing in human cells occurs via the Fanconi anemia pathway. *Nat Genet* 2018;50:1132–1139. DOI: 10.1038/s41588-018-0174-0.
8. Chen F, Pruett-Miller SM, Huang Y, et al. High-frequency genome editing using ssDNA oligonucleotides with zinc-finger nucleases. *Nat Methods* 2011;8:753–755. DOI: 10.1038/nmeth.1653.
9. DeWitt MA, Magis W, Bray NL, et al. Selection-free genome editing of the sickle mutation in human adult hematopoietic stem/progenitor cells. *Sci Transl Med* 2016;8:360ra134. DOI: 10.1126/scitranslmed.aaf9336.
10. Richardson CD, Ray GJ, DeWitt MA, et al. Enhancing homology-directed genome editing by catalytically active and inactive CRISPR-Cas9 using asymmetric donor DNA. *Nat Biotechnol* 2016;34:339–344. DOI: 10.1038/nbt.3481.
11. Roth TL, Puig-Saus C, Yu R, et al. Reprogramming human T cell function and specificity with non-viral genome targeting. *Nature* 2018;559:405–409. DOI: 10.1038/s41586-018-0326-5.
12. Okamoto S, Amaishi Y, Maki I, et al. Highly efficient genome editing for single-base substitutions using optimized ssODNs with Cas9-RNPs. *Sci Rep* 2019;9:4811. DOI: 10.1038/s41598-019-41121-4.

13. Liang X, Potter J, Kumar S, et al. Enhanced CRISPR/Cas9-mediated precise genome editing by improved design and delivery of gRNA, Cas9 nuclease, and donor DNA. *J Biotechnol* 2017;241:136–146. DOI: 10.1016/j.jbiotec.2016.11.011.
14. Orlando SJ, Santiago Y, DeKelver RC, et al. Zinc-finger nuclease-driven targeted integration into mammalian genomes using donors with limited chromosomal homology. *Nucleic Acids Res* 2010;38:e152. DOI: 10.1093/nar/gkq512.
15. Bedell VM, Wang Y, Campbell JM, et al. *In vivo* genome editing using a high-efficiency TALEN system. *Nature* 2012;491:114–118. DOI: 10.1038/nature11537.
16. Li M, Zhao L, Page-McCaw PS, et al. Zebrafish genome engineering using the CRISPR-Cas9 system. *Trends Genet* 2016;32:815–827. DOI: 10.1016/j.tig.2016.10.005.
17. Ceasar SA, Rajan V, Prykhozhij SV, et al. Insert, remove or replace: a highly advanced genome editing system using CRISPR/Cas9. *Biochim Biophys Acta* 2016;1863:2333–2344. DOI: 10.1016/j.bbamcr.2016.06.009.
18. Paix A, Folkmann A, Goldman DH, et al. Precision genome editing using synthesis-dependent repair of Cas9-induced DNA breaks. *Proc Natl Acad Sci U S A* 2017;114:E10745–E10754. DOI: 10.1073/pnas.1711979114.
19. Boel A, De Saffel H, Steyaert W, et al. CRISPR/Cas9-mediated homology-directed repair by ssODNs in zebrafish induces complex mutational patterns resulting from genomic integration of repair-template fragments. *Dis Model Mech* 2018;11:dmm035352. DOI: 10.1242/dmm.035352.
20. Aird EJ, Lovendahl KN, St Martin A, et al. Increasing Cas9-mediated homology-directed repair efficiency through covalent tethering of DNA repair template. *Commun Biol* 2018;1:54. DOI: 10.1038/s42003-018-0054-2.
21. Savic N, Ringnalda FC, Lindsay H, et al. Covalent linkage of the DNA repair template to the CRISPR-Cas9 nuclease enhances homology-directed repair. *eLife* 2018;7:e33761. DOI: 10.7554/eLife.33761.
22. Komor AC, Kim YB, Packer MS, et al. Programmable editing of a target base in genomic DNA without double-stranded DNA cleavage. *Nature* 2016;533:420–424. DOI: 10.1038/nature17946.
23. Gaudelli NM, Komor AC, Rees HA, et al. Programmable base editing of A*T to G*C in genomic DNA without DNA cleavage. *Nature* 2017;551:464–471. DOI: 10.1038/nature24644.
24. Anzalone AV, Randolph PB, Davis JR, et al. Search-and-replace genome editing without double-strand breaks or donor DNA. *Nature* 2019;576:149–157. DOI: 10.1038/s41586-019-1711-4.
25. Park J, Lim K, Kim J-S, et al. Cas-analyzer: an online tool for assessing genome editing results using NGS data. *Bioinformatics* 2016;33:286–288. DOI: 10.1093/bioinformatics/btw561.
26. Ma AC, McNulty MS, Poshusta TL, et al. FusX: a rapid one-step transcription activator-like effector assembly system for genome science. *Hum Gene Ther* 2016;27:451–463. DOI: 10.1089/hum.2015.172.
27. Cunliffe VT. Zebrafish: a practical approach. Edited by C. Nüsslein-Volhard and R. Dahm. Oxford University Press. 2002. 322 pages. ISBN 0 19 963808 X. Price £40.00 (paperback). ISBN 0 19 963809 8. Price £80.00 (hardback). *Genet Res* 2003;82:79–79. DOI: 10.1017/S0016672303216384.
28. Hyatt TM, Ekker SC. Vectors and techniques for ectopic gene expression in zebrafish. *Methods Cell Biol* 1999;59:117–126. DOI: 10.1016/s0091-679x(08)61823-3.
29. Hsiau T, Conant D, Rossi N, et al. Inference of CRISPR edits from Sanger trace data. *bioRxiv* 2019;251082. DOI: 10.1101/251082.
30. Papapetrou EP, Schambach A. Gene insertion into genomic safe harbors for human gene therapy. *Mol Ther* 2016;24:678–684. DOI: 10.1038/mt.2016.38.
31. Cong L, Ran FA, Cox D, et al. Multiplex genome engineering using CRISPR/Cas systems. *Science* 2013;339:819–823. DOI: 10.1126/science.1231143.
32. Brinkman EK, Chen T, Amendola M, et al. Easy quantitative assessment of genome editing by sequence trace decomposition. *Nucleic Acids Res* 2014;42:e168. DOI: 10.1093/nar/gku936.
33. Glaser A, McColl B, Vadolas J. GFP to BFP conversion: a versatile assay for the quantification of CRISPR/Cas9-mediated genome editing. *Mol Ther Nucleic Acids* 2016;5:e334. DOI: 10.1038/mtna.2016.48.
34. Krug II RG, Poshusta TL, Skuster KJ, et al. A transgenic zebrafish model for monitoring glucocorticoid receptor activity. *Genes Brain Behav* 2014;13:478–487. DOI: 10.1111/gbb.12135.
35. Lee HB, Schwab TL, Sigafoos AN, et al. Novel zebrafish behavioral assay to identify modifiers of the rapid, nongenomic stress response. *Genes Brain Behav* 2019;18:e12549. DOI: 10.1111/gbb.12549.
36. Jao L-E, Wente SR, Chen W. Efficient multiplex biallelic zebrafish genome editing using a CRISPR nuclease system. *Proc Natl Acad Sci U S A* 2013;110:13904–13909. DOI: 10.1073/pnas.1308335110.
37. Paul B, Montoya G. CRISPR-Cas12a: Functional overview and applications. *Biomed J* 2020;43:8–17. DOI: 10.1016/j.bj.2019.10.005.
38. Walton RT, Christie KA, Whittaker MN, et al. Unconstrained genome targeting with near-PAMless engineered CRISPR-Cas9 variants. *Science* 2020;368:290–296. DOI: 10.1126/science.aba8853.
39. Nemudryi AA, Valetdinova KR, Medvedev SP, et al. TALEN and CRISPR/Cas genome editing systems: tools of discovery. *Acta Naturae* 2014;6:19–40.
40. Lamb BM, Mercer AC, Barbas CF 3rd. Directed evolution of the TALE N-terminal domain for recognition of all 5′ bases. *Nucleic Acids Res* 2013;41:9779–9785. DOI: 10.1093/nar/gkt754.
41. Ma AC, Lee HB, Clark KJ, et al. High efficiency *in vivo* genome engineering with a simplified 15-RVD GoldyTALEN design. *PLoS One* 2013;8:e65259. DOI: 10.1371/journal.pone.0065259.
42. Feng Y, Zhang S, Huang X. A robust TALENs system for highly efficient mammalian genome editing. *Sci Rep* 2014;4:3632. DOI: 10.1038/srep03632.
43. Renaud J-B, Boix C, Charpentier M, et al. Improved genome editing efficiency and flexibility using modified oligonucleotides with TALEN and CRISPR-Cas9 nucleases. *Cell Rep* 2016;14:2263–2272. DOI: 10.1016/j.celrep.2016.02.018.
44. Ma AC, McNulty MS, Poshusta TL, et al. FusX: a rapid one-step transcription activator-like effector assembly system for genome science. *Hum Gene Ther* 2016;27:451–463. DOI: 10.1089/hum.2015.172.
45. Gratz SJ, Cummings AM, Nguyen JN, et al. Genome engineering of Drosophila with the CRISPR RNA-guided Cas9 nuclease. *Genetics* 2013;194:1029–1035. DOI: 10.1534/genetics.113.152710.
46. Hoshijima K, Jurynec MJ, Grunwald DJ. Precise editing of the zebrafish genome made simple and efficient. *Dev Cell* 2016;36:654–667. DOI: 10.1016/j.devcel.2016.02.015.
47. Boel A, De Saffel H, Steyaert W, et al. CRISPR/Cas9-mediated homology-directed repair by ssODNs in zebrafish induces complex mutational patterns resulting from genomic integration of repair-template fragments. *Dis Model Mech* 2018;11:dmm035352. DOI: 10.1242/dmm.035352.
48. Kato GJ, Piel FB, Reid CD, et al. Sickle cell disease. *Nat Rev Dis Primers* 2018;4:18010. DOI: 10.1038/nrdp.2018.10.